

Tight-binding calculations of the band structure and total energies of the various phases of magnesium

H. J. Gotsis, D. A. Papaconstantopoulos, and M. J. Mehl

Code 6390, Center for Computational Materials Science, Naval Research Laboratory, Washington, DC 20375

(Received 16 October 2001; published 15 March 2002)

Tight-binding calculations for Mg in a variety of crystal structures are reported using the nonorthogonal tight-binding model with parameters selected to fit accurately first-principles results. These parameters correctly predict hcp to be the stable crystal structure. We have calculated electronic properties (band structure and density of states), elastic constants, phonon frequencies at high-symmetry points, surface energies, surface electronic structure, stacking fault energies, the energy of a small cubic cluster, and finally, dynamical properties. We find good agreement with previous calculations and experiment.

DOI: 10.1103/PhysRevB.65.134101

PACS number(s): 71.10.-w, 68.35.Md, 73.20.At, 62.20.Dc

I. INTRODUCTION

The electronic structure of hcp metals has been discussed previously by several authors.¹⁻⁵ In particular, Mg is an important alkaline-earth element existing in many compounds. While most hcp materials do not have the ideal value of the ratio $c/a = \sqrt{8/3} \approx 1.633$, magnesium has the ratio $c/a = 1.623$, which is very close to ideal one and has, therefore, attracted much interest. In addition to this, the bulk modulus⁶ of 35.4 GPa caused Mg to be regarded as a “soft” metal and thus elastic constant calculations pose a theoretical challenge.

The full-potential linear-augmented-plane-wave (FP-LAPW) (Refs. 7,8) method has been employed with electronic structure calculations of all hcp metals up to cadmium.¹ In particular, the density of states of Mg compares well with augmented-plane-wave² and pseudopotential calculations,³ whereas difference electron densities show almost no deviation from spherical symmetry. Band structures, densities of states, and Fermi surfaces for Mg, Zn, and Cd have been calculated using the linear muffin-tin orbitals (LMTO) method.⁴ The large variation in the c/a ratio between the near ideal in Mg and the far from ideal in Zn and Cd allows for interesting comparisons of their electronic structures and Fermi surfaces. In the case of Mg, the total density of states below the Fermi level is a “free-electron-gas” parabola, in sharp contrast with the density of states for Zn and Cd, where there is a significant contribution from the d states. The electronic and structural properties of hcp Mg have been calculated at the Hartree-Fock level, the hybrid Hartree-Fock–density-functional level and the density-functional level within the local-density and generalized gradient approximations.⁵ Comparison shows that various properties of Mg, such as elastic constants, can be accounted for within the Kohn-Sham schemes, especially when nonlocal correlation and exchange potentials are used, provided that d functions are included in the basis set.⁵

There is an approach completely different from the previous ones, called the spherical cellular method, which replaces the Wigner-Seitz polyhedron by a sphere.⁹ The main goal was to investigate the numerical properties of the cellular method and validate its accuracy against established re-

sults. It was found that the spherical cellular method works well for alkali metals, but for fcc Mg the agreement with the calculations of Moruzzi, Janak, and Williams¹⁰ was only fair. Phonon-dispersion curves have been calculated for hcp Mg, using first-principles pseudopotentials.^{11,12} The calculated curves are in fair agreement with experiment.

In another type of calculation, using force model methods,¹³ the calculated phonon dispersions are compared with inelastic neutron-scattering data and good agreement is found. The surface energy and the surface dipole barrier of simple metals have been calculated by application of the Kohn-Sham energy functional of the density with the inclusion of an exchange and correlation correction to account for the inhomogeneity of the electron gas.¹⁴ The surface energy is minimized with respect to two parameters, describing the decrease of the electron density at the surface and the relaxation of the top lattice plane. For the fcc Mg(111) surface the calculated values are in good agreement with the experimental ones and are better than the jellium model values of Ref. 15. Surface energies of simple metals have been computed by application of the Rayleigh-Ritz variational principle to the Kohn-Sham energy functional of the density.¹⁶ For most of the simple metals examined, the variational bounds are superior to perturbation-theory results,¹⁵ whereas for Mg variational and perturbative results are approximately the same. The corrected effective medium method was applied to the calculation of the surface energy of a variety of metal surfaces.¹⁷ For the perfectly terminated hcp Mg(1000) surface the agreement with experiment is very good. Chemisorption properties have been calculated for adsorbate Mg on Mg surfaces, using the effective medium theory.¹⁸ In addition, calculated values for the surface energy of the free Mg(0001) and Mg(11 $\bar{2}$ 0) surfaces are presented, all in fair agreement with available experimental and other theoretical values.

The surface electronic structure of Mg(0001) has been calculated using a self-consistent pseudopotential approach.¹⁹ The surface states were determined for a ten-layer Mg film and are in good agreement with angle-resolved photoemission experiments.^{20,21} Finnis-Sinclair-type many-body potentials have been constructed for eight hcp metals, which reproduce the observed c/a ratio and the elastic con-

stants for each metal considered.²² Using the constructed potentials, the stacking fault energies on the basal plane have been calculated. For some elements the stacking fault energy is high, whereas for others it is unphysically low. However, it is in the experimentally expected range for Mg. The modified embedded-atom method, an empirical extension of embedded-atom method that includes angular forces, has been applied to hcp metals.²³ Calculated stacking fault energies and surface energies were found to be in reasonable agreement with experiment. The energetics of various stacking defects in hcp Mg were determined from first-principles local-density-approximation calculations.²⁴ The energies of these defects suggest that Mg is likely to form stacking faults with the two kinds of intrinsic fault I_1 and I_2 , being the most probable defects. Based on the first-principles results, a local bond orientation model is proposed that is able to predict the energies of arbitrary stacking sequences. Stacking fault and surface energies have been calculated for ten hcp metals using the embedded-atom methodology.²⁵ The calculated surface energies for the basal and prism planes of Mg are about equal and both are less than the experiment. The two kinds of intrinsic faults I_1 and I_2 , and the extrinsic fault E have energies that are much lower than those reported by others. However, reasonable stacking fault energies have been obtained for Mg.

In this paper we use the NRL-TB method,²⁶ a nonorthogonal tight-binding method, in the two-center representation that uses environmentally dependent parameters obtained from fitting *ab initio* calculations of a few high-symmetry structures, to compute the electronic structure of the various phases of magnesium. The method produces good structural energy differences, elastic constants, phonon frequencies, vacancy formation energies, and surface energies for the alkaline-earth, transition, and noble metals.²⁶ We find that the results predict hcp Mg as the stable crystal structure, consistent with experiment. This increases our confidence that the reason for the correct results in the tested configurations is that the underlying physics of the model is sound.

The paper is organized as follows: In Sec. II, we describe the functional form of our TB parametrization and the fitting data set. In Sec. III, we discuss applications of the TB model to a range of properties such as the ground-state electronic structure of the various phases of Mg, band structure and density of states, elastic constants, phonon frequencies, surface energies, surface electronic structure, stacking fault energies, and the energy of an eight-atom Mg cluster. In addition, we performed molecular-dynamics (MD) simulations at various temperatures to obtain the temperature dependence of the atomic mean-square displacement and of the pressure. In Sec. IV, we summarize the results.

II. FUNCTIONAL FORM AND FITTING

In this paper we present results for a tight-binding parametrization using an sp^3d^5 basis. This set of parameters allows all interactions between p and d orbitals, in order to account for the p - d hybridized bands above the Fermi level (E_F). Since the functional forms of the parameters used in the NRL

scheme have already been presented,²⁶ we will only give a brief summary here. The total energy of the system is written as the sum of the energies of the occupied electronic eigenstates. The onsite Hamiltonian matrix elements vary with the local density associated with each atom, allowing the NRL-TB method to use in the fit LAPW eigenvalues that have been shifted so that the LAPW total energy is equal to the eigenvalue sum. Therefore, all of the contributions to the total energy are accounted for in the eigenvalue sum and the addition of a sum of pair potentials, a feature common to most TB models, is not needed.

The energies of the electronic states and the corresponding eigenvectors are the solutions of a generalized eigenvalue equation with Hamiltonian and overlap matrix elements parametrized as follows: the basis used to describe the Hamiltonian and overlap matrices is a set of one s , three p , and five d orbitals around each atom, with all interactions between atoms assumed to be in the two-center approximation.²⁷ A local atomic density at atom i is defined as

$$\rho_i = \sum_j e^{-\lambda^2 |\mathbf{R}_j - \mathbf{R}_i|} f(|\mathbf{R}_j - \mathbf{R}_i|), \quad (1)$$

where \mathbf{R}_i is the position of atom i and λ is a fitting parameter. The cutoff function $f(R)$ is given by

$$f(R) = \begin{cases} \left[1 + \exp\left(\frac{R - R_c + 5l}{l}\right) \right]^{-1}, & R \leq R_c \\ 0, & R > R_c, \end{cases} \quad (2)$$

where R_c is 16.5 a.u. and l is 0.5 a.u.. The onsite matrix elements are given in terms of the local atomic density ρ_i as

$$h_{ii} = \alpha_i + \beta_l \rho_i^{2/3} + \gamma_l \rho_i^{4/3} + \chi_l \rho_i^2, \quad (3)$$

where l is the orbital-type index (s , p or d), and α_l , β_l , γ_l , and χ_l are fitting parameters. The distance dependence of the two-center hopping matrix elements is given by

$$H_{ll'\mu}(R) = (a_{ll'\mu} + b_{ll'\mu}R + c_{ll'\mu}R^2) \exp(-g_{ll'\mu}^2 R) f(R), \quad (4)$$

where l and l' are orbital-type indices, μ is an index for the type of interaction between orbitals (σ , π or δ), and the parameters $a_{ll'\mu}$, $b_{ll'\mu}$, $c_{ll'\mu}$, and $g_{ll'\mu}$ are fitting parameters. The overlap matrix elements have the same functional form as the Hamiltonian matrix elements. The angular dependence of the Hamiltonian and overlap matrix elements is the standard two-center Slater-Koster form.²⁷

The 97 parameters used by the functional form for the sp^3d^5 basis parametrization are fit to four high-symmetry crystal structures.²⁸ The fitting data set includes both the total energy and band structure for the simple cubic (sc), face-centered cubic (fcc), body-centered cubic lattice (bcc), and only energy bands for the hexagonal close-packed (hcp) structure, for a wide range of volumes around the energy minimum. The total energy and eigenvalues of each crystal were computed by linear augmented-plane-wave,^{7,8} *ab initio* density-functional theory calculations in the generalized gra-

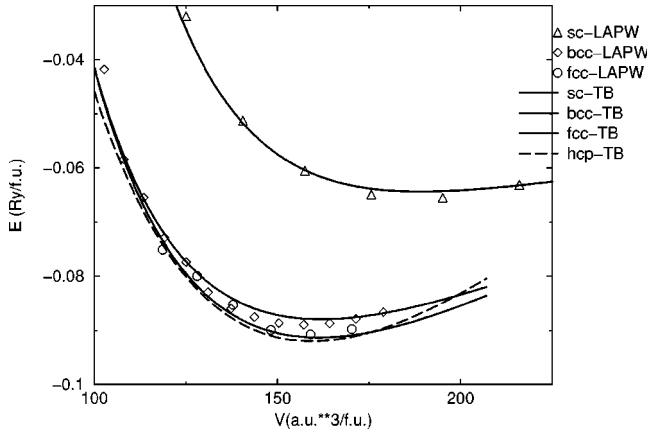


FIG. 1. Total energy vs volume for a number of crystal structures as well as the hcp structure for Mg (not included in the fit), computed using the TB model.

dient approximation (DFT/GGA).²⁹ The sc lattice data included the widest range of volumes, from 125.0 to 216.0 $\text{\AA}^3/\text{atom}$. The fcc lattice structures ranged from 118.6 to 170.4 $\text{\AA}^3/\text{atom}$, the bcc lattice from 119.2 to 171.5 $\text{\AA}^3/\text{atom}$, and the hcp lattice from 135.0 to 156.9 $\text{\AA}^3/\text{atom}$.

III. APPLICATIONS

A. Static calculations

We started total-energy calculations using parameters obtained by fitting to muffin-tin (MT) augmented-plane-wave results. The MT approximation led to sizable errors, for example, the calculated elastic constants were up to 100% too large. Therefore, we decided to fit FP-LAPW results for all total-energy calculations presented in this paper. Several band-structure calculations of Mg exist in the literature,^{1,4,5} in comparison to these calculations we found some differences at points *M* and *K* of the Brillouin zone. A treatment of symmetry in the fitting procedure gave the correct features of the Mg band structure at these points.

The ground-state total energies as a function of volume for a range of structures are shown in Fig. 1. The TB model reproduces the LAPW results very well for the fcc, bcc, and sc structures to which it was fit, and predicts the correct ground state to be the hcp structure, the total energy of which was not included in the fit. The root-mean-square (rms) error of the bands for all the structures is 19.0 mRy for the lowest four bands and the rms error for the total energies is 1.4 mRy. The TB calculations predict equilibrium lattice parameters $a = 3.22 \text{ \AA}$ and $c = 5.26 \text{ \AA}$, in excellent agreement with the experimental ones of 3.21 and 5.21 \AA , respectively.

The band structure of hcp Mg along directions of high crystal symmetry is shown in Fig. 2. A striking feature of the Mg band structure is that it can be well described by the parabolic dependence of a free-electron gas. This similarity to the free-electron gas is characteristic of simple metals such as Mg. The TB band structure is very similar to previous ones.^{1,4,5} The FP-LAPW,¹ the LMTO (Ref. 4) and the DFT/GGA (Ref. 5) band structures are all reminiscent of the free-electron one.

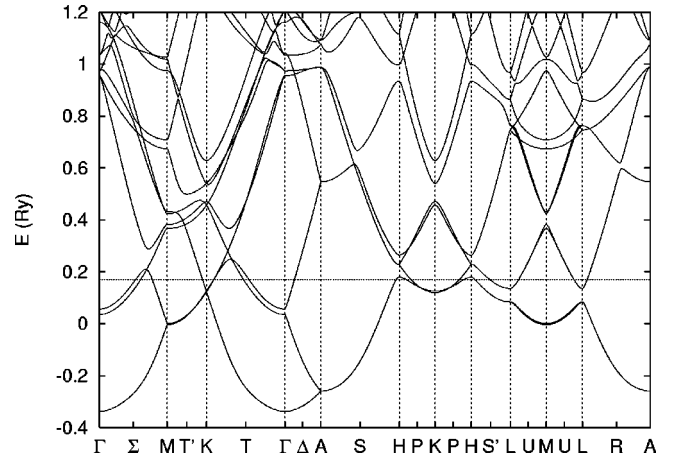


FIG. 2. Band structure along high-symmetry directions in the Brillouin zone for hcp Mg.

The relationship between the TB band structure and the corresponding density of states (DOS) is demonstrated in Fig. 3. One cannot fail to notice the distinct similarity to the free-electron-gas parabolic density of states. The partial DOS functions show that the strongest contribution to the total DOS comes from the *p* bands.

The elastic constants C_{ij} contain some of the most important information that can be obtained from ground-state total-energy calculations. A given crystal structure cannot exist in a stable or metastable phase unless its elastic constants obey certain relationships. The C_{ij} also determine the response of the crystal to external forces and so play an important part in determining the strength of a material. The procedure for calculating elastic constants from first-principles calculations is described by Mehl, Klein, and Papaconstantopoulos.³⁰ The same procedure is used in our TB calculations. Briefly, one imposes an external strain on the crystal and calculates the energy as a function of strain. Our method predicts correctly the bulk modulus, whereas it gives reasonable elastic constants, as shown in Table I. The agreement between our calculated values and the experimental data is satisfactory (within 26% for C_{11} , 29% for C_{12} , 36% for C_{33} , and 24% for C_{44}). As a general rule, the off-diagonal elastic constants

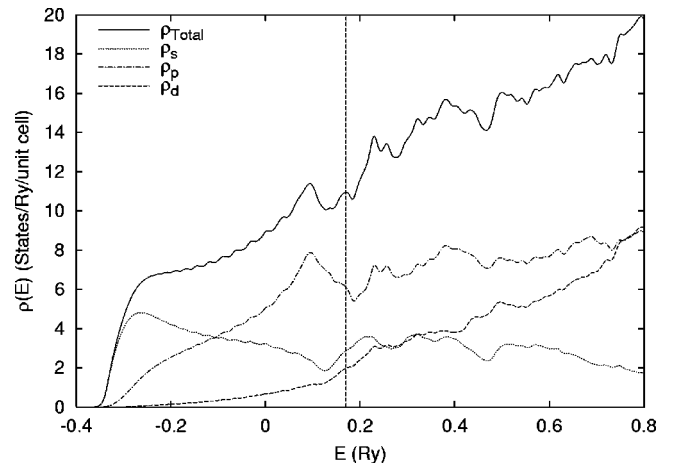


FIG. 3. Total and partial densities of states for hcp Mg.

TABLE I. Elastic constants and bulk modulus in GPa for magnesium in the hcp structure, computed with the sp^3d^5 TB model; comparison with experimental data.

	TB	Expt. ^a
c_{11}	79.98	63.48
c_{12}	18.33	25.94
c_{13}	5.23	21.70
c_{33}	90.48	66.45
c_{44}	22.77	18.42
B^b	34.46	35.4

^aFrom Ref. 31.

^bExperimental value from Ref. 6.

such as C_{13} are affected by larger errors and poor agreement for the C_{13} value (within 76%) is expected. Since Mg is a soft metal, we calculated elastic constants using different k -point meshes, and found that they are very sensitive to the number of k points. Comparison of our results with the Kohn-Sham models of Ref. 5, shows that the Becke-Perdew scheme with the inclusion of d functions leads to values very close to experimental ones. However, our GGA functionals²⁹ are different from the Becke-Perdew exchange-correlation functionals.

Phonon frequencies at high-symmetry points in the Brillouin zone (BZ) computed with the TB model using the frozen-phonon approximation are compared with experimentally measured values in Table II. For some phonons the agreement is quite good (within 17% for Γ_5^+ , 32% for M_3^+ , 23% for M_3^- , 34% for M_2^+ , and 26% for M_2^-), whereas for other modes the agreement is poor.

Magnesium surfaces are modeled using a slab geometry and converged with respect to the number of atoms in the slab. Surface energies are calculated by deriving a bulk energy by subtracting energies of two slabs with n and m atoms. The difference between the energy of the slab and the energy of the bulk is the surface energy

$$E_{\text{surface}} = \frac{1}{2} [E_{\text{slab}}(n) - E_{\text{bulk}}n], \quad (5)$$

TABLE II. Phonon frequencies (in THz) at high-symmetry points of the BZ computed with the TB model and measured experimentally.

	TB	Expt. ^a
Γ_5^+	4.34	3.70
Γ_3^+	12.11	7.30
M_4^+	9.99	3.70
M_3^+	5.46	4.15
M_3^-	6.73	5.45
M_2^+	4.35	6.58
M_2^-	8.66	6.88
A_1	7.11	2.94
A_3	3.19	5.20

^aFrom Ref. 12.

TABLE III. Surface energies of Mg (0001), (1000), $(\bar{1}100_a)$, and $(\bar{1}100_b)$ surfaces, in units of J/m^2 .

	TB	Expt. ^a
(0001)	0.95	0.785
(1000)	1.20	
$(\bar{1}100_a)$	1.06	
$(\bar{1}100_b)$	1.36	

^aAverage of a polycrystalline surface, Ref. 32.

where E_{surface} is the energy associated with one unit cell on the surface of the slab. In Table III, we display surface energies of unrelaxed and unreconstructed Mg surfaces. The (0001) surface is perpendicular to the z direction and is the close-packed surface of the hcp structure. The (1000) surface is perpendicular to the x direction and is not as close packed as the (0001). From Table III we observe that the surface energy in the (0001) surface is lower than in (1000), as generally the most close-packed surface has the lowest surface energy. The $(\bar{1}100)$ surface is perpendicular to the y direction and has two possible truncations. The $(\bar{1}100_a)$ represents atoms with z coordinate $+c/4$, whereas $(\bar{1}100_b)$ represents atoms with z coordinate $-c/4$. Due to unavailability of experimental data on isolated surfaces, comparison with experiment is only semiquantitative. The experimental value is an average over various Mg faces extrapolated to zero temperature³² and the agreement with our calculated values can be regarded as satisfactory.

The surface electronic structure of Mg(0001) is calculated using a bulk terminated (0001) surface hcp slab with 30 atoms. We define surface states as states whose wave function is concentrated up to 10% on the surface layer. This definition is not a rigorous one and introduces an ambiguity in the identification of surface states. Figure 4 shows the band structure of the (0001) surface hcp slab. One surface band is located in the upper part of the valence band at M in agreement with previous theoretical¹⁹ and experimental works.^{20,21}

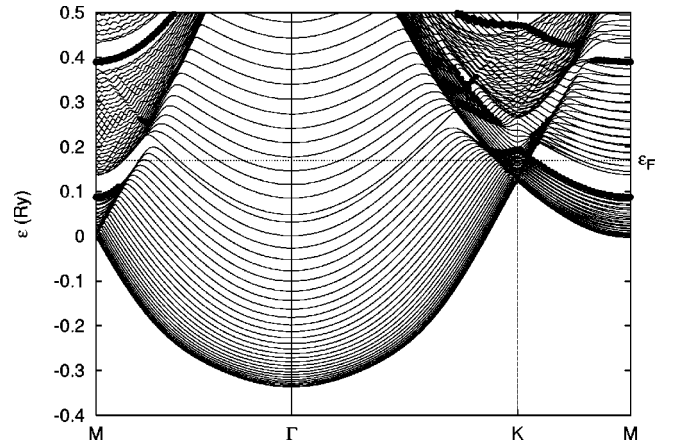


FIG. 4. Surface band structure of Mg(0001). Surface states are represented by filled circles, whereas bulk bands are represented by curves.

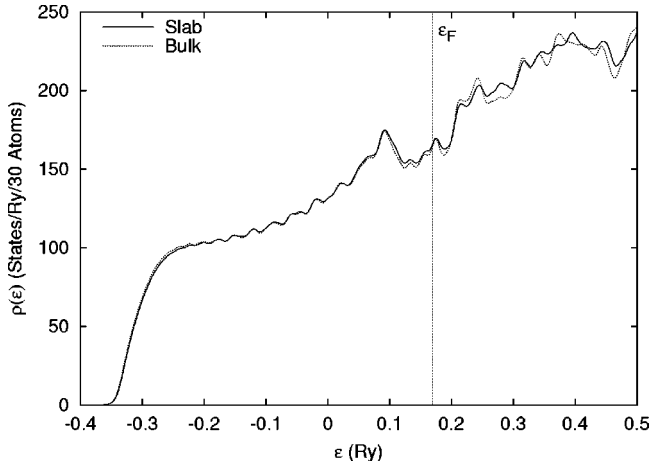


FIG. 5. Total slab and bulk densities of states for Mg(0001).

Furthermore, analysis of our results shows that there is another surface state at Γ with energy -1.65 eV relative to the Fermi level. This surface state is in excellent agreement with the experimental value -1.6 eV (Ref. 21) and the theoretical value -1.56 eV.¹⁹ In Fig. 5 we compare the total slab and bulk densities of states. The bulk density of states is the partial DOS from a middle atom scaled by a factor of 30. The deviation between slab and bulk densities of states is due to the surface states bands.

In close-packed metals, such as Mg, planar defects are formed with relative ease, contributing to the ductile nature of these materials. It is well known that crystals glide on the densest atomic planes; for Mg the basal plane is the densest and the primary slip system is basal. We calculate stacking fault energies as a function of the displacement in the $[2010]$ direction along the (0001) plane. We assume that relaxations are negligible and the atoms in the faulted region maintain a close-packed coordination.³³ In Fig. 6 we show the stacking fault energy as a function of the stacking fault variable q . The unstable stacking fault energy γ_{us} is the peak of the curve, whereas the intrinsic stacking fault energy γ_{is} is the

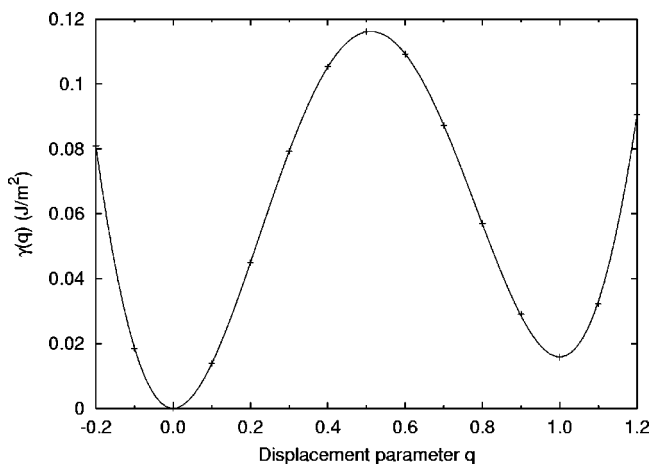


FIG. 6. Stacking fault energy as a function of the stacking displacement q for hcp Mg, determined by the NRL-TB method. At $q=0$ there is no stacking fault, at $q=1$ we reach the intrinsic stacking fault energy (a local fcc-like crystal structure).

TABLE IV. The unstable stacking fault energy γ_{us} , the intrinsic stacking fault energy γ_{is} , and the ductility parameter D of Mg. The values of γ_{us} and γ_{is} were obtained from a polynomial fit to the points in Fig. 6. γ_{us} and γ_{is} are in units of J/m^2 .

γ_{us}	γ_{is}	D
0.116	0.016	2.46

local minimum on the right of the curve. Using the formation energy for the (0001) surface and the unstable stacking fault energy, we calculate the Rice ductility parameter D .³⁴ The results are shown in Table IV. We observe that the ductility parameter is greater than one, consistent with the intrinsic ductility of Mg.

To test the transferability of our parameters we compute the total energy of a small cluster. In our approach, we take the cluster as a finite part of the infinite crystalline solid and determine the equilibrium size for this fixed structure. The structure we consider is an eight-atom Mg cube in a large simple cubic unit cell. We construct a huge unit cell, a cube 100 bohr on a side, and keep the atoms near the origin so that they do not interact with their periodic replicas. The only neighbors are the atoms in the immediate cluster. In Fig. 7 we present the cluster energy as a function of interatomic distance, starting from 7.9 down to 7.1 bohr. The minimum separation is 7.397 bohr, substantially greater than the bulk separation of 6.047 bohr.⁶

B. MD simulations

Our MD simulations use the tight-binding molecular-dynamics (TBMD) code,³⁵ which is based on a quantum-mechanical description of the interatomic interactions. In the MD simulations, the system consists of an hcp supercell of 288 atoms. The equations of motion were integrated using a time step of 2 fs for 2000 steps. We performed MD simulations for several temperatures at the experimental lattice constants, $a=3.21$ Å and $c=5.21$ Å, to compute the atomic mean-square displacement and then the Debye-Waller factor. In Fig. 8 we compare the temperature dependence of our

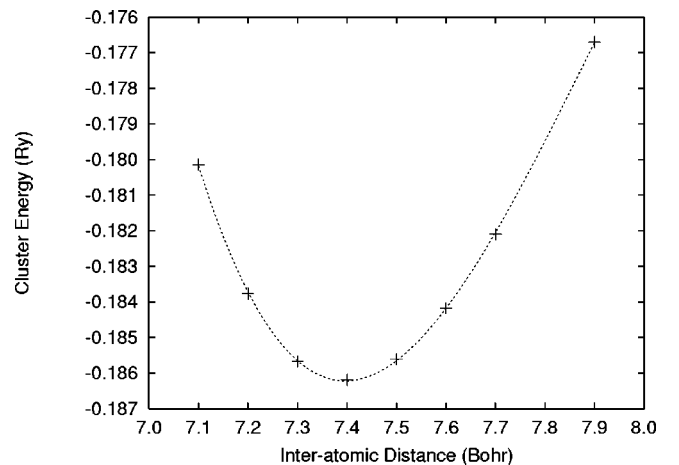


FIG. 7. TB parametrization for an eight-atom Mg cube.

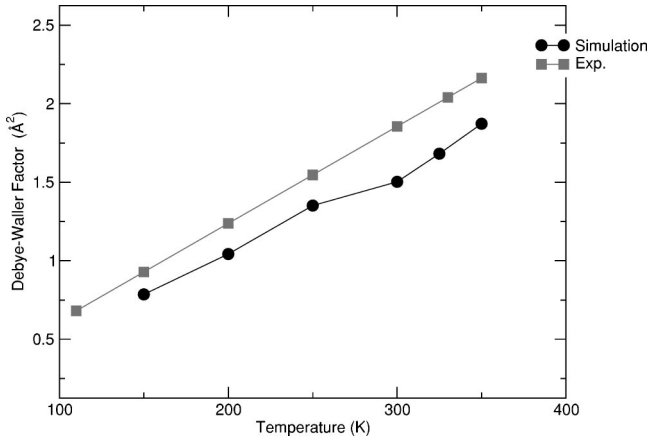


FIG. 8. Debye-Waller factor of Mg as a function of temperature. The filled circles are the results of the molecular-dynamics simulations using our TB model, filled squares are the experimental points (Ref. 36).

computed Debye-Waller factor with experimental data.³⁶ The overall agreement with experiment is good, given that our calculated values are well within 19% of experiment in the temperature range we simulated. The melting temperature of Mg was calculated from Lindemann's criterion.³⁷ According to this criterion, at the melting temperature the average amplitude of vibration is about 15% of the nearest-neighbor distance. A linear extrapolation of our atomic mean-square displacement results gives a melting temperature of 824 K, consistent with the experimental value of 922 K.⁶

To determine the theoretical thermal-expansion coefficient α we use the following definition for α :

$$\alpha = \frac{1}{3B} \left(\frac{\partial P}{\partial T} \right)_V. \quad (6)$$

This definition requires the calculation of the pressure as a function of temperature for a fixed volume. We perform MD simulations at 150, 200, 250, 300, 325, and 350 K, keeping the volume fixed at the experimental value. The c/a ratio is taken to be the experimental one. For each temperature we select ten configurations from the trajectories generated by the MD simulations and compute the pressure. In Fig. 9 we show pressure as a function of temperature as derived from the simulations. From Fig. 9 we can see that it is reasonable to assume that the pressure varies linearly as a function of temperature. In Eq. 6, if for the bulk modulus B we use the theoretical and the experimental values (taken from Table I), we get $\alpha = 7.12 \times 10^{-6}$ and $6.93 \times 10^{-6} \text{ K}^{-1}$, respectively. These values underestimate the experimental value of $\alpha = 25 \times 10^{-6} \text{ K}^{-1}$ at 300 K.³⁸

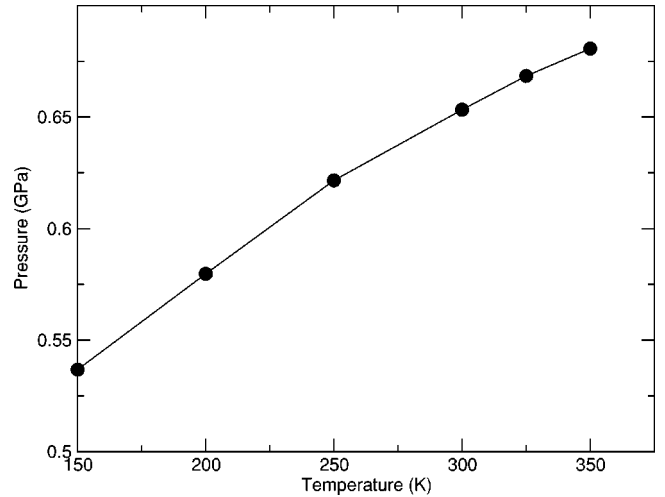


FIG. 9. Pressure as a function of temperature for Mg, derived from molecular-dynamics simulations using our TB model.

IV. SUMMARY

We have applied the NRL-TB method to generate a TB model for Mg that was fit to LAPW results of a small number of high-symmetry crystal structures. We found that the resulting Hamiltonian is transferable to a wider range of geometries. This model with a nonorthogonal sp^3d^5 basis reproduces experimental measurements for a range of material properties, such as elastic constants and phonon frequencies. It correctly describes slabs as approximate systems for surfaces. This TB model also describes the energy of a small isolated cluster for different interatomic distances. In addition, we performed molecular-dynamics simulations at various temperatures to compute the Debye-Waller factor and the thermal-expansion coefficient. Both quantities were found to be in good agreement with experimental data. The ability of the model to accurately describe such diverse properties and systems, despite having been fitted to only a small number of high-symmetry crystal structures, increases our confidence that it captures the essential physics of bonding in magnesium systems.

ACKNOWLEDGMENTS

This work was supported by the U.S. Office of Naval Research and the Common High Performance Computing Software Support Initiative (CHSSI) of the United States Department of Defense High Performance Computing Modernization Program (HPCMP). The work of H.J.G. was supported by the National Research Council Associateship Program. One of us (H.J.G.) would like to thank Dr. N. Bernstein for assistance with the NRL TB-MD package.

¹P. Blaha, K. Schwarz, and P. H. Dederichs, Phys. Rev. B **38**, 9368 (1988).

²S. T. Inoue and J. Yamashita, J. Phys. Soc. Jpn. **35**, 677 (1973).

³P. Rennert, H. Schelle, and U. H. Glaser, Phys. Status Solidi B

121, 673 (1984).

⁴S. Daniuk, T. Jarlborg, G. Kontrym-Sznajd, J. Majsnerowski, and H. Stachowiak, J. Phys.: Condens. Matter **1**, 8397 (1989).

⁵I. Baraille, C. Pouchan, M. Causà, and F. Marinelli, J. Phys.:

- Condens. Matter **10**, 10 969 (1998).
- ⁶Charles Kittel, *Introduction to Solid State Physics*, 7th ed. (Wiley, New York, 1996).
- ⁷O. K. Andersen, Phys. Rev. B **12**, 3060 (1975).
- ⁸S. H. Wei and H. Krakauer, Phys. Rev. Lett. **55**, 1200 (1985).
- ⁹M. Farjam and H. B. Shore, Phys. Rev. B **37**, 1059 (1988).
- ¹⁰V. L. Moruzzi, J. F. Janak, and A. R. Williams, *Calculated Electronic Properties of Metals* (Pergamon, New York, 1978).
- ¹¹D. Sen, Phys. Rev. B **42**, 1217 (1990).
- ¹²F. Marinelli, M. Roche, I. Baraille, and C. Pouchan, Phys. Rev. B **54**, 6054 (1996).
- ¹³M. Li, J. Phys.: Condens. Matter **13**, 1907 (2001).
- ¹⁴G. Paasch and M. Hietschold, Phys. Status Solidi B **67**, 743 (1975).
- ¹⁵N. D. Lang and W. Kohn, Phys. Rev. B **1**, 4555 (1970).
- ¹⁶V. Sahni and J. Gruenebaum, Phys. Rev. B **19**, 1840 (1979).
- ¹⁷T. J. Raeker and A. E. DePristo, Phys. Rev. B **39**, 9967 (1989).
- ¹⁸Z. J. Tian, U. Yxklinten, B. I. Lundqvist, and K. W. Jacobsen, Surf. Sci. **258**, 427 (1991).
- ¹⁹E. V. Chulkov, V. M. Silkin, and E. N. Shirykalov, Surf. Sci. **188**, 287 (1987).
- ²⁰U. O. Karlsson, G. V. Hansson, P. E. S. Persson, and S. A. Flodström, Phys. Rev. B **26**, 1852 (1982).
- ²¹R. A. Bartynski, R. H. Gaylord, T. Gustafsson, and E. W. Plummer, Phys. Rev. B **33**, 3644 (1986).
- ²²M. Igarashi, M. Khantha, and V. Vitek, Philos. Mag. B **63**, 603 (1991).
- ²³M. I. Baskes and R. A. Johnson, Model. Simul. Mater. Sci. Eng. **2**, 147 (1994).
- ²⁴N. Chetty and M. Weinert, Phys. Rev. B **56**, 10 844 (1997).
- ²⁵Wangyu Hu, Bangwei Zhang, Baiyun Huang, Fei Gao, and David J. Bacon, J. Phys.: Condens. Matter **13**, 1193 (2001).
- ²⁶R. E. Cohen, M. J. Mehl, and D. A. Papaconstantopoulos, Phys. Rev. B **50**, 14 694 (1994); M. J. Mehl and D. A. Papaconstantopoulos, *ibid.* **54**, 4519 (1996); in *Topics in Computational Materials Science*, edited by C. Y. Fong (World Scientific, Singapore, 1998).
- ²⁷W. A. Harrison, *Electronic Structure and the Properties of Solids* (Dover, New York, 1989).
- ²⁸The NRL-TB parameters used in this study for magnesium are available at http://cst-www.nrl.navy.mil/bind/mg_par
- ²⁹J. P. Perdew, J. A. Chevary, S. H. Vosko, K. A. Jackson, M. R. Pederson, D. J. Singh, and C. Fiolhais, Phys. Rev. B **46**, 6671 (1992).
- ³⁰M. J. Mehl, Phys. Rev. B **47**, 2493 (1993); M. J. Mehl, B. A. Klein, and D. A. Papaconstantopoulos, in *Intermetallic Compounds: Principles and Applications*, edited by J. H. Westbrook and R. L. Fleischer (Wiley, London, 1994), Vol. 1, Chap. 9.
- ³¹G. Simmons and H. Wang, *Single Crystal Elastic Constants and Calculated Aggregate Properties: A Handbook*, 2nd ed. (MIT, Cambridge, MA, 1971).
- ³²W. R. Tyson and W. A. Miller, Surf. Sci. **62**, 267 (1977).
- ³³M. J. Mehl, D. A. Papaconstantopoulos, N. Kioussis, and M. Herbranson, Phys. Rev. B **61**, 4894 (2000).
- ³⁴J. R. Rice, J. Mech. Phys. Solids **40**, 239 (1992).
- ³⁵F. Kirchhoff, M. J. Mehl, N. I. Papanicolaou, D. A. Papaconstantopoulos, and F. S. Khan, Phys. Rev. B **63**, 195101 (2001).
- ³⁶L. M. Peng, G. Ren, S. L. Dudarev, and M. J. Whelan, Acta Crystallogr., Sect. A: Found. Crystallogr. **52**, 456 (1996).
- ³⁷F. A. Lindemann, Z. Phys. **11**, 609 (1910).
- ³⁸Y. S. Touloukian, in *A Physicist's Desk Reference: The Second Edition of the Physics Vade Mecum*, edited by H. L. Anderson (American Institute of Physics, New York, 1989), p. 345.